molecules

MDPI

Communication

Facile Preparation of Porous Carbon Derived from Pomelo Peel for Efficient Adsorption of Methylene Blue

Wenlin Zhang [1,2], Mingwan Liu [1], Yuhong Zhao [3] and Qinhong Liao [1,*]

1 Chongqing Key Laboratory of Economic Plant Biotechnology, College of Landscape Architecture and Life Science (Institute of Special Plants), Chongqing University of Arts and Sciences, Yongchuan, Chongqing 402160, China; zhangwenlin88519@126.com (W.Z.); chocolate11702@126.com (M.L.)
2 College of Food Science, Southwest University, Beibei, Chongqing 400716, China
3 College of Biology and Food Engineering, Chongqing Three Gorges University, Wanzhou, Chongqing 404199, China; zyh0101hyz@163.com
* Correspondence: lqhwisdom@cqwu.edu.cn

Abstract: Pomelo peel waste-derived porous carbon (PPPC) was prepared by a facile one-step $ZnCl_2$ activation method. The preparation parameters of PPPC were the mass ratio of $ZnCl_2$ to pomelo peel of 2:1, carbonization temperature of 500 °C, and carbonization time of 1 h. This obtained PPPC possessed abundant macro-,meso-, and micro-porous structures, and a large specific surface area of 939.4 $m^2\ g^{-1}$. Surprisingly, it had excellent adsorption ability for methylene blue, including a high adsorption capacity of 602.4 mg g^{-1} and good reusability. The adsorption isotherm and kinetic fitted with Langmuir and pseudo-second order kinetic models. This work provides a novel strategy for pomelo peel waste utilization and a potential adsorbent for treating dye wastewater.

Keywords: porous carbon; pomelo peel; adsorbent; methylene blue

Citation: Zhang, W.; Liu, M.; Zhao, Y.; Liao, Q. Facile Preparation of Porous Carbon Derived from Pomelo Peel for Efficient Adsorption of Methylene Blue. *Molecules* **2022**, *27*, 3096. https://doi.org/10.3390/molecules27103096

Academic Editors: Guohui Dong, Na Chen and Wei Liu

Received: 19 April 2022
Accepted: 9 May 2022
Published: 11 May 2022

1. Introduction

Organic dye wastewater produced from textile, printing, leather, and paper industries becomes a serious pollution problem once it is discharged into the environment without effective treatment [1]. Methylene blue (MB) is a commonly used dye in these industries and has potential toxicities for aquatic environments and humans [2,3]. Importantly, MB molecule in wastewater is difficult to decompose under natural conditions [4]. Therefore, removing MB from wastewater is urgently necessary.

According to previous reports, many techniques such as adsorption, membrane filtration, biodegradation, photocatalysis, chemical oxidation, and so on, have been used to treat dye wastewater [5]. Among these methods, adsorption is a competitive approach owing to its low cost and easy operation [6]. Porous carbon has many applications in wastewater treatment, electrochemical uses, and medicine [7,8]. Particularly, it is a very promising adsorbent for organic dye removal, attributed to its highly specific surface area and abundant hierarchical pore structures [9]. Previous studies reported that the macropores in porous carbon could promote the mass transfer process, and the mesopores and micropores could catch MB molecules [10,11]. Recently, several porous carbons derived from various biomass raw materials such as ficus carica bast, coconut leaves, and palm shell were developed as adsorbents for MB removal [12–14]. However, it is still necessary to seek abundant and low-cost biomass sources to prepare porous carbons with good adsorption performance.

Pomelo is widely planted in the south of China and is consumed freshly or processed in large amounts annually. Pomelo peel (PP) accounts for half of fresh fruit weight, which is mostly discarded as waste in juice or jam-processing industries [15]. Seriously, it can cause a series of environmental problems and the wastage of pomelo resources. In addition, PP has a sponge-like mesh porous structure and contains abundant cellulose (46.22%) and hemicellulose (18.84%) [16]. Therefore, using PP as a raw material to prepare porous carbon material is worth considering. Liu et al. prepared PP-derived porous carbon with a BET-specific surface area of 832 m^2 g^{-1} by the combination of hydrothermal carbonization and KOH activation at 700 °C for 2 h [17]. Li et al. synthesized porous carbon by the pre-carbonization of PP at 450 °C and followed by KOH activation and carbonization at 800 °C [18]. Although its BET-specific surface area can reach up to 1892.10 m^2 g^{-1}, the carbonization time (t) is up to 6 h. It can be found that the above steps are tedious, time consuming, and involve high energy consumption. Moreover, KOH could cause serious corrosion to the synthesis equipment. Herein, PP-derived porous carbon (PPPC) was developed by a one-step $ZnCl_2$ activation method (Figure 1), and their adsorption ability and reusability for MB was evaluated.

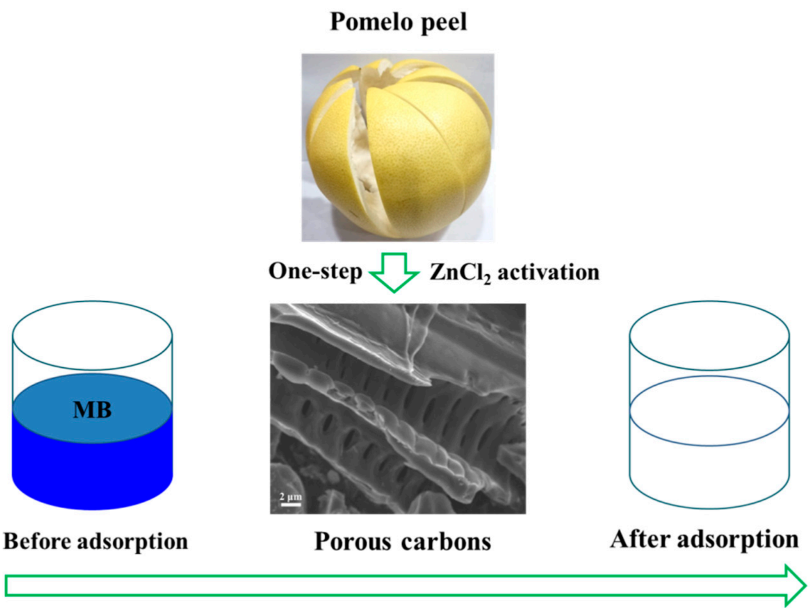

Figure 1. Illustration of the synthesis and adsorption application of PPPC.

2. Materials and Methods

2.1. Materials

The mature 'Liangpingyou' pomelos were obtained from a pomelo orchard in Liangping District, Chongqing, China, and their peels were subsequently dried, smashed, and sieved through a 60-mesh sieve. MB were purchased from Sigma-Aldrich Co. LLC. (St Louis, MO, USA). Other chemicals of analytical reagent grade were obtained from Chengdu Kelong Chemical Reagent Co. (Chengdu, Sichuan, China). Ultrapure water was used for all experiments.

2.2. Preparation of PPPC

In a typical process, 1.0 g PP powder and 0.5–4 g $ZnCl_2$ were added into 50 mL water under vigorous stirring for 2 h. Subsequently, the mixtures were freeze-dried. The dried mixtures were transferred in a tube furnace and heated at 300–700 °C under nitrogen flow with a rate of 5 °C min^{-1} for 0.5–2.5 h. Then, the prepared samples were washed with 1 mol L^{-1} HCl solution and water, respectively. Finally, the products were dried at 60 °C in an oven.

2.3. Material Characterizations

The morphology of PPPC was observed by a JEOL JSM-7100F field-emission scanning electron microscope (FESEM, Tokyo, Japan) operated at 10 kV. Nitrogen adsorption-desorption isotherm was measured using a Quadrasorb instrument (Quantachrome, Boynton Beach, FL, USA) at 150 °C, and the data analysis was performed with Quantachrome software. X-ray diffraction (XRD) patterns were studied using a Rigaku Ultima IV X-ray diffractometer with Cu-Kα radiation (λ = 0.15418 nm). Fourier transform-infrared (FTIR) spectrum was recorded using a Nicolet 6700 spectrophotometer (Thermo Fisher, Cleveland, OH, USA). Raman spectrum was performed by a DXR Raman spectroscopy system (Thermo Fisher, Cleveland, OH, USA). Zeta potential was determined using a Malvern Zetasizer Nano ZS 90 spectrometer.

2.4. Adsorption and Regeneration Experiments

Adsorption experiments were performed in glass bottles containing 5.0 mg PPPC and 10 mL MB aqueous solutions with various initial concentrations. Subsequently, the mixtures were shaken at 200 rpm with different pH, time, and temperature, respectively. Then, the samples were centrifuged and the supernatant concentrations were determined by a UV-Vis spectrophotometer at 664 nm. For the effect of pH on the adsorption, the different calibration curves were used to determine MB concentration at different pH. The equations of MB adsorption capacity, pseudo-first-order kinetic, pseudo-second-order kinetic, Langmuir, and Freundlich models were listed as follows.

$$q_e = \frac{(c_0 - c_e)V}{m} \tag{1}$$

$$\log(q_e - q_t) = \log q_e - \frac{k_1 t}{2.303} \tag{2}$$

$$\frac{t}{q_t} = \frac{1}{k_2 q_e^2} + \frac{t}{q_e} \tag{3}$$

$$\frac{c_e}{q_e} = \frac{c_e}{q_m} + \frac{1}{b q_m} \tag{4}$$

$$\log q_e = \log k + \frac{1}{n} \log c_e \tag{5}$$

where, q_e (mg g^{-1}) is the equilibrium adsorption capacity; c_0 (mg L^{-1}) and c_e (mg L^{-1}) are the initial and equilibrium concentrations of MB, respectively; V (L) is solution volume; m (g) is the mass of PPPC; q_t (mg g^{-1}) is the adsorption capacity at any time; k_1(min^{-1}) and k_2 (g mg^{-1} min^{-1}) are the kinetics adsorption rate constants; t is contact time (min); q_m (mg g^{-1}) is the maximum adsorption capacity; b (L mg^{-1}) is the adsorption constant; k is the indicator of adsorption capacity; and $1/n$ is the heterogeneity factor.

For the regeneration study, 5.0 mg of PPPC was added to 10 mL MB solution (100 mg L^{-1}) at pH 12 and the mixtures were shaken at 200 rpm for 2 h at 25 °C. After adsorption and centrifugation, the supernatant was discarded leaving PPPC. Then, MB-adsorbed PPPC was added to 10 mL pH = 2 ethanol and shaken at 200 rpm for 10 min. Subsequently, PPPC was isolated from the solution by centrifugation and used for the next cycle. The final concentration of MB was determined by UV-vis spectra. The adsorption-desorption processes were conducted five times.

3. Results and Discussion

3.1. Synthesis of PPPC

In the study, PPPC was successfully prepared by a one-step $ZnCl_2$ activation method. To obtain PPPC with better adsorption performance for MB, the mass ratio of $ZnCl_2$ to PP (MRZP), carbonization temperature (T), and t were optimized by one-factor-at-a-time approach (OFAT). As shown in Figure 2A, q_e of PPPC increased with the increasing MRZP until 2:1, and reached the highest of 397.4 mg g^{-1} for 2:1. Subsequently, it decreased when MRZP was over 2:1. According to previous reports, it was considered that impregnation with suitable $ZnCl_2$ could make PP undergo oxidative degradation and catalytic dehydration during the carbonization process, which led to aromatization and charring of carbon skeleton and formed more pores to improve the q_e [19]. In addition, q_e of PPPC increased sharply with the increasing T from 300 °C to 500 °C and reached a maximum of

394.4 mg g^{-1} at 500 °C. However, it decreased when T was over 500 °C (Figure 2B). This was probably because the higher temperature (600 and 700 °C) could destroy the pore structures of PPPC and caused the decrease of specific surface area [17], which led to the decrease of q_e. Moreover, with the extension of t until 1 h, q_e of PPPC increased gradually (Figure 2C) and reached the highest value of 398.18 mg g^{-1} at 1 h. Then, q_e showed a decreasing trend over 1 h. It was found that appropriate MRZP, T, and t could improve the adsorption performance of PPPC greatly. Therefore, MRZP of 2:1, T of 500 °C, and t of 1 h were chosen as the optimum preparation parameters of PPPC.

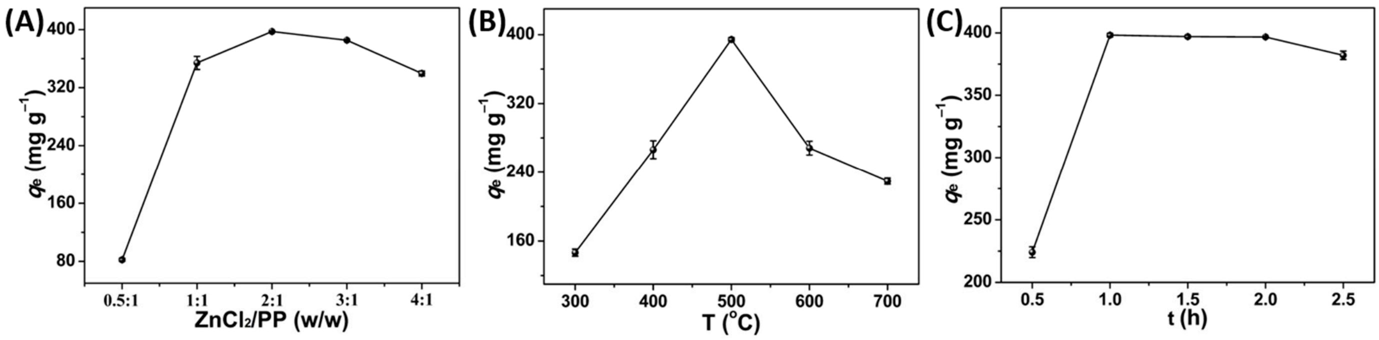

Figure 2. Effect of (**A**) MRZP (T: 500 °C, t: 1 h), (**B**) T (MRZP: 2:1, t: 1 h), and (**C**) t (MRZP: 2:1, T: 500 °C) for MB adsorption on PPPC (pH: 12, c_0: 200 g L^{-1}, 2 h, 25 °C).

3.2. Characterizations of PPPC

FESEM image in Figure 3A showed that the optimized PPPC possessed rich and uniform macropores. To further investigate the mesopore and micropore characteristics as well as the specific surface area of PPPC, the nitrogen adsorption-desorption isotherm was performed. As seen in Figure 3B, the isotherm increased sharply at a low relative pressure of $P/P_0 < 0.05$, suggesting that PPPC had abundant micropores [20]. Subsequently, a hysteresis loop appeared on the isotherm of PPPC at $0.4 < P/P_0 < 1.0$, indicating the existence of many mesopores in PPPC [20]. Moreover, the pore size distribution result also proved that PPPC possessed rich micropores and mesopores (Figure 3C). The total pore volume and average pore diameter of PPPC were 0.62 cm^3 g^{-1} and 2.6 nm. Together with SEM analysis, PPPC indeed had abundant porous structures. Notably, these porous structures not only make MB molecules enter PPPC surface quickly, but also entrap and adsorb more MB molecules to improve the adsorption capacity of PPPC [11]. Particularly, the specific surface area of PPPC was up to 939.4.2 m^2 g^{-1}, and it was larger than those of previously reported porous carbons (Table S1), except the KOH-activated PP-based porous carbon (1892.1 m^2 g^{-1}).

XRD pattern was employed for exploring the structure and phase composition of PPPC. The broad two peaks at 25.4° and 43.3° corresponded to the (002) and (101) planes of the disordered carbon layer (Figure 3D), indicating that the carbon with a turbostratic structure with low crystallinity existed in PPPC [21]. According to the previous report, the turbostratic structures were beneficial for the adsorption of dye molecules [22]. Moreover, the low angle region ($2\theta < 15°$) appeared to have high intensity, which was ascribed to the abundant micropores in PPPC [11,21], which confirmed the results of nitrogen adsorption-desorption isotherm and size distribution studies. Raman spectrum showed that the peaks at 1586 cm^{-1} (G-band) and 1334 cm^{-1} (D-band) corresponded to the ordered graphitic carbon and lattice defects carbon in PPPC [23] (Figure 3E), respectively. Furthermore, the I_D/I_G ratio was calculated to be 0.89, revealing the existence of rich disordered carbons in PPPC. In addition, the full width at half maximum (FWHM) of the D band was obviously wider than that of the G band, indicating a high percentage of disorder and defects in the carbons [21], which was in agreement with the XRD result. FTIR spectrum was used to study the surface organic groups of PPPC. As shown in Figure 3F, the bands at 3458 and 3315 cm^{-1}; 2923 and 2854 cm^{-1}; 1869 cm^{-1}; 1614 and 1567 cm^{-1}; 1153 and 1074 cm^{-1}; and 889 and 802 cm^{-1}, represented –OH, $-CH_2$, C=O, C=C, C–O, and C-H groups respectively, which were derived from the carbonization of PP during the carbonization process [3,20]. Based on the above results, it was known that many oxygenated groups existed on the surface of PPPC. To be emphasized, these oxygenated groups were critical for MB adsorption due to the interactions and offered numerous adsorption sites [13].

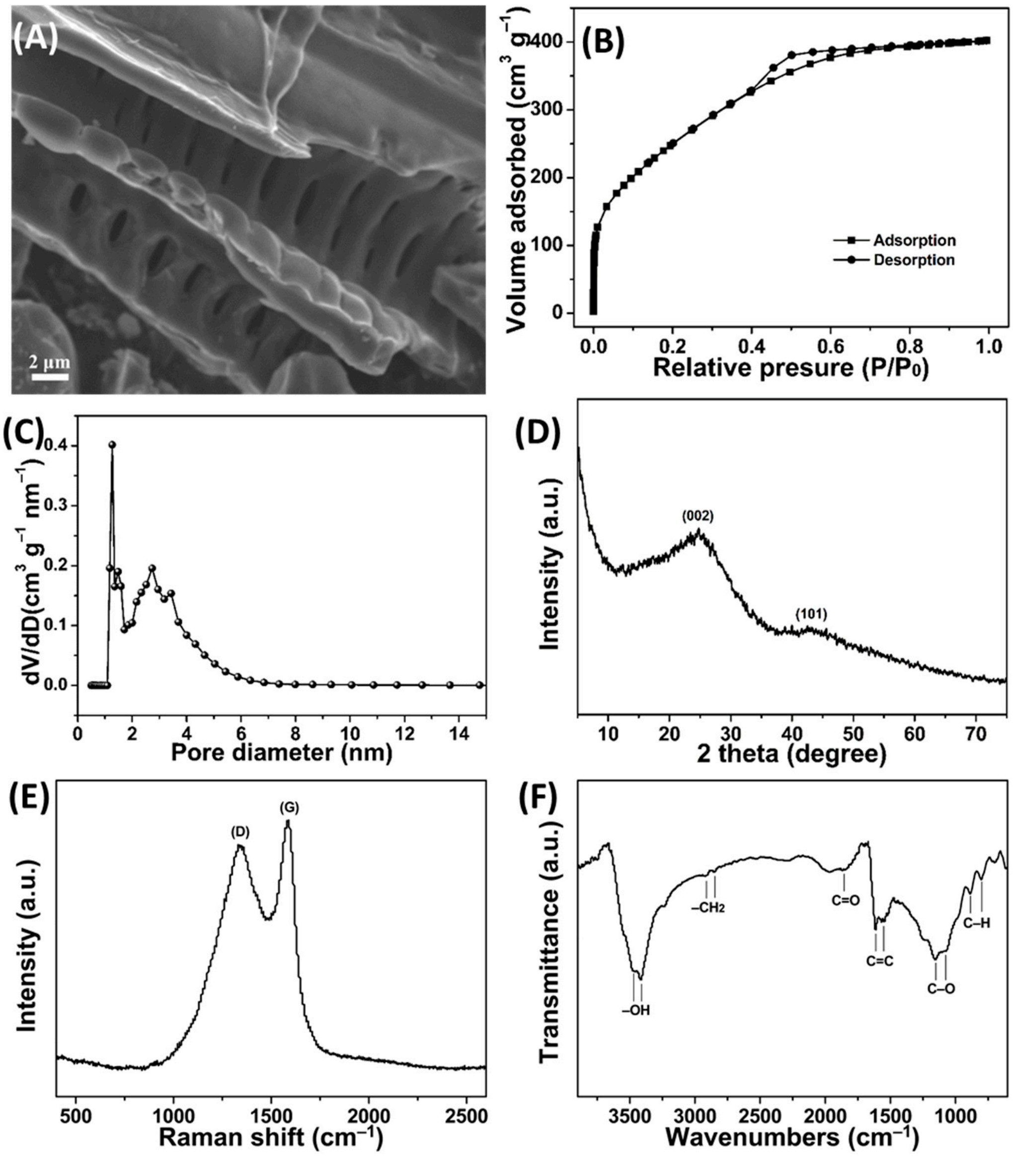

Figure 3. (**A**) SEM image, (**B**) nitrogen adsorption–desorption isotherm, (**C**) pore size distribution, (**D**) XRD pattern, (**E**) Raman, and (**F**) FTIR spectra of PPPC.

3.3. Adsorption Performance of PPPC

For MB dye adsorption, pH is an important influencing factor [24]. It was seen that the q_e increased from 261.7 mg g^{-1} to 393.6 mg g^{-1} as pH raised from 2 to 12 (Figure 4A). According to the result, the surface charge of PPPC was negatively charged above pH 3.2 (pH_{pzc} = 3.2, Figure S1A), owed to the surface functional groups including hydroxyl and carboxyl [25], and MB is positively charged [26]. With the pH rise, the enhanced electrostatic interaction between PPPC and MB resulted in a higher q_e [12]. In addition, q_e improved with the increased c_0 (Figure S1B), suggesting higher c_0 could provide a stronger driving force to promote the mass transfer of MB [27]. Moreover, q_e increased with the raised adsorption temperature (Figure S1C), suggesting the adsorption process was endothermic [28]. Figure 4B showed that the adsorption was fast (302.2 mg g^{-1} min^{-1}) within 1 min because of the abundant vacant adsorption sites. Then, the rate dropped, owing to the repulsive force between adsorbed dye molecules on PPPC and free dye molecules in aqueous solution [29]. Finally, the adsorption system was at equilibrium at 60 min with q_e of 549.6 mg g^{-1}. It can be found that the adsorption was a rapid process, which was beneficial for the practical application of PPPC.

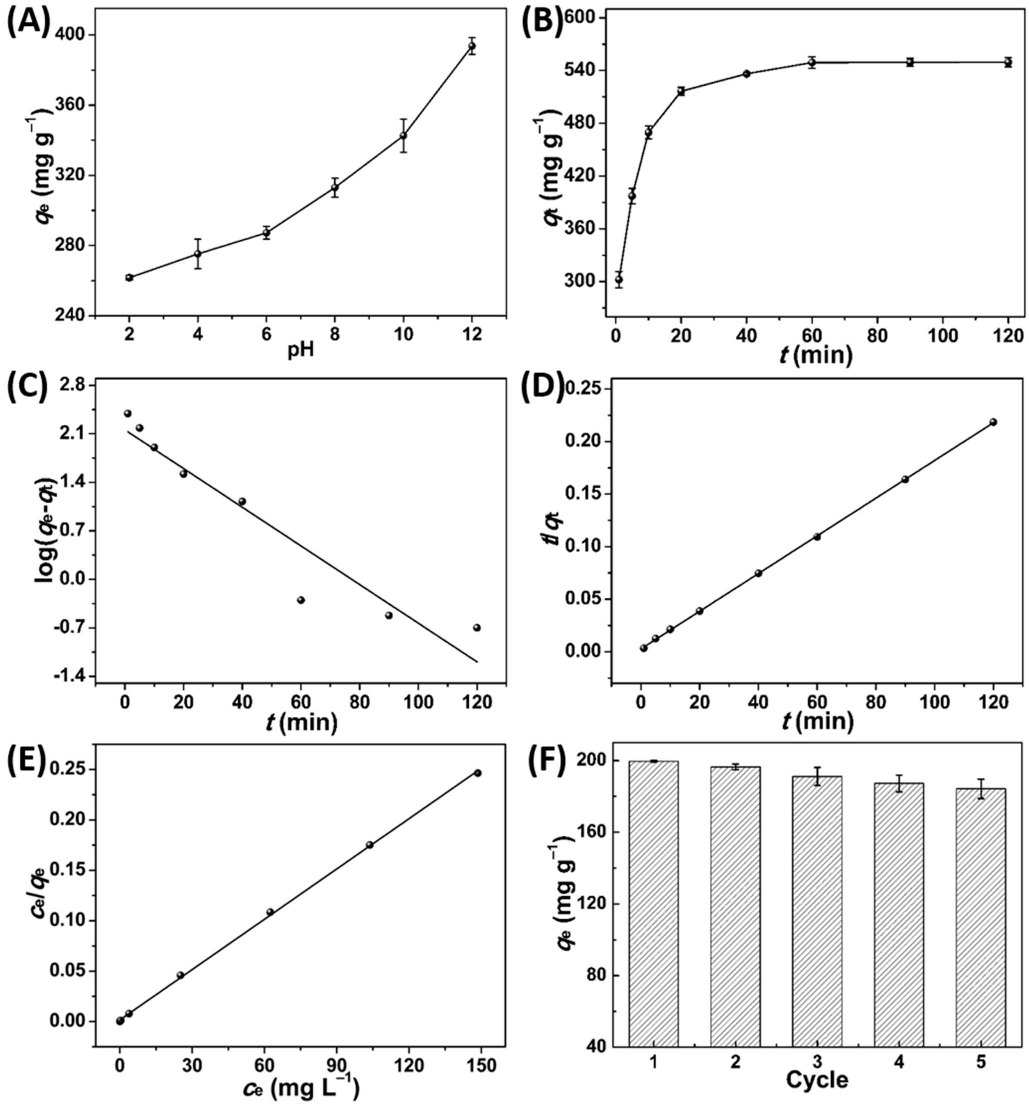

Figure 4. Effect of (**A**) pH (c_0: 200 g L^{-1}, 2 h, 25 °C); (**B**) t (c_0: 200 g L^{-1}, pH: 12, 25 °C); (**C**) pseudo-first order kinetic; (**D**) pseudo-second order kinetic; (**E**) Langmuir isotherm of MB adsorption on PPPC; and (**F**) the reusability of PPPC toward MB adsorption (c_0: 100 g L^{-1}, pH: 12).

The pseudo-first-order kinetic and pseudo-second-order kinetic were applied to analyze the equilibrium kinetic data (Figure 4C,D; Table 1). It was shown that R^2 (0.9999) of the pseudo-second order kinetic was higher than R^2 (0.8973) of the pseudo-first order kinetic, and its calculated equilibrium adsorption capacity ($q_{e,cal}$ = 558.7 mg g^{-1}) was consistent with the experimental equilibrium adsorption capacity ($q_{e,exp}$ = 549.6 mg g^{-1}). This suggested that the adsorption process was well depicted by the pseudo-second order kinetic and involved the chemisorption [30]. To quantitatively study the maximum adsorption capacity (q_m) and the characteristics of adsorption of MB by PPPC, Langmuir and Freundlich isotherms were employed. As shown in Figure 4E and Figure S1D, and Table 2, R^2 (0.9995) of Langmuir isotherm was much higher than R^2 (0.8327) of Freundlich isotherm, indicating the adsorption process obeyed Langmuir isotherm [31]. This revealed that the adsorption of MB by PPPC was mainly a monolayer adsorption, which was consistent with the previously reported porous carbons with similar pore structures [12,32,33]. Based on Langmuir isotherm, the calculated q_m was 602.4 mg g^{-1}, which was larger than those of various adsorbents (Table S2). In addition, the recyclability of PPPC is crucial for its application value. Figure 4F showed that q_e only reduced by 7.7% after five cycles, suggesting that PPPC had good reusability for removing MB dye. According to our previous report [12], the stable structure of PPPC might be the main reason for its good reusability.

Table 1. Pseudo-first order and pseudo-second order kinetics parameters.

Pseudo-First-Order Kinetics					Pseudo-Second-Order Kinetics		
c_0 (mg L^{-1})	$q_{e,exp}$ (mg g^{-1})	$q_{e,cal}$ (mg g^{-1})	k_1 (min^{-1})	R^2	$q_{e,cal}$ (mg g^{-1})	k_2 (g mg^{-1} min^{-1})	R^2
300	549.6	143.4	0.06	0.8973	558.7	0.0012	0.9999

Table 2. Langmuir and Freundlich isotherms parameters.

Langmuir			Freundlich		
q_m (mg g^{-1})	b (L mg^{-1})	R^2	k	$1/n$	R^2
602.4	1.02	0.9995	298.33	0.17	0.8327

The possible adsorption mechanism of PPPC toward MB was summarized. Adsorption is a complicated physicochemical phenomenon related to interphase mass-transfer, surface interactions, intraparticle diffusion, and so on [34]. The excellent adsorption ability of PPPC was attributed to its abundant pores, which could reduce hindrance to accelerate the mass transfer process and capture more MB molecules [12]. Meanwhile, the electrostatic interaction and H-bonding interaction between PPPC and MB caused by the rich function groups of PPPC could influence the adsorption performance [3,10,35]. Furthermore, the π-π interaction generated by the aromatic structures of PPPC and MB was beneficial for MB adsorption [10]. From the analysis of pseudo-second order kinetic and the desorbed MB amount (Figure S2), it can be inferred that chemisorption also existed in the adsorption process. In summary, the adsorption mechanism was due to the combined effect of physisorption and chemisorption.

4. Conclusions

Pomelo peel-derived porous carbon with large specific surface area and abundant pore structures were prepared by a facile one-step method. The porous carbon had high adsorption capacity and excellent reusability toward MB, and the adsorption process obeyed Langmuir and pseudo-second order kinetic models. The work opened a new approach for pomelo peel utilization and a potential absorbent for wastewater treatment.

Supplementary Materials: The following are available online at https://www.mdpi.com/article/10.3390/molecules27103096/s1. Figure S1: (A) Zeta potential of PPPC at different pH. Effect of (B) $c0$ and (C) T for MB adsorption on PPPC and (D) Freundlich isotherm for MB adsorption on PPPC. Figure S2: The desorbed MB concentrations in ethanol for five cycles. Table S1: The specific surface area of various porous carbon materials. Table S2: The q_m of various adsorbents [3,6,17,18,36–47].

Author Contributions: W.Z. supplied the research idea and completed the experiments; M.L. and Y.Z. analyzed the data; Q.L. managed the experiments and wrote the paper. All authors have read and agreed to the published version of the manuscript.

Funding: This study was supported by Natural Science Foundation Project of Chongqing (cstc2019jcyj-msxmX0819) and Innovation and Entrepreneurship Training program for College Students (S202110642017).

Data Availability Statement: Not applicable.

Conflicts of Interest: The authors have no conflict of interest.

References

1. Lu, K.; Wang, T.; Zhai, L.; Wu, W.; Dong, S.; Gao, S.; Mao, L. Adsorption behavior and mechanism of Fe-Mn binary oxide nanoparticles: Adsorption of methylene blue. *J. Colloid Interface Sci.* **2019**, *539*, 553–562. [CrossRef] [PubMed]
2. Rezakazemi, M.; Shirazian, S. Lignin-chitosan blend for methylene blue removal: Adsorption modeling. *J. Mol. Liq.* **2019**, *274*, 778–791. [CrossRef]
3. Zhang, W.; Li, H.; Tang, J.; Lu, H.; Liu, Y. Ginger straw waste-derived porous carbons as effective adsorbents toward methylene blue. *Molecules* **2019**, *24*, 469. [CrossRef] [PubMed]
4. Mustafa, I. Methylene blue removal from water using H_2SO_4 crosslinked magnetic chitosan nanocomposite beads. *Microchem. J.* **2019**, *144*, 397–402.
5. Rashid, R.; Shafiq, I.; Akhter, P.; Iqbal, M.J.; Hussain, M. A state-of-the-art review on wastewater treatment techniques: The effectiveness of adsorption method. *Environ. Sci. Pollut. Res.* **2021**, *28*, 9050–9066. [CrossRef] [PubMed]
6. He, K.; Zeng, G.; Chen, A.; Huang, Z.; Peng, M.; Huang, T.; Chen, G. Graphene hybridized polydopamine-kaolin composite as effective adsorbent for methylene blue removal. *Compos. Part B Eng.* **2019**, *161*, 141–149. [CrossRef]
7. Zhang, Y.; Yang, L.; Yan, L.; Wang, G.; Liu, A. Recent advances in the synthesis of spherical and nanoMOF-derived multifunctional porous carbon for nanomedicine applications. *Coordin. Chem. Rev.* **2019**, *391*, 69–89. [CrossRef]
8. Yu, M.; Han, Y.; Li, J.; Wang, L. CO_2-activated porous carbon derived from cattail biomass for removal of malachite green dye and application as supercapacitors. *Chem. Eng. J.* **2017**, *317*, 493–502. [CrossRef]
9. Zhang, Y.; Ji, G.; Li, C.; Wang, X.; Li, A. Templating synthesis of hierarchical porous carbon from heavy residue of tire pyrolysis oil for methylene blue removal. *Chem. Eng. J.* **2020**, *390*, 124398. [CrossRef]
10. Zhang, L.Y.; Zhang, W.; Zhou, Z.; Li, C.M. γ-Fe_2O_3 nanocrystals-anchored macro/meso-porous graphene as a highly efficient adsorbent toward removal of methylene blue. *J. Colloid Interface Sci.* **2016**, *476*, 200–205. [CrossRef]
11. Zhang, W.; Zhang, L.Y.; Zhao, X.J.; Zhou, Z. Citrus pectin derived porous carbons as a superior adsorbent toward removal of methylene blue. *J. Solid State Chem.* **2016**, *243*, 101–105. [CrossRef]
12. Wong, K.T.; Eu, N.C.; Ibrahim, S.; Kim, H.; Yoon, Y.; Jang, M. Recyclable magnetite-loaded palm shell-waste based activated carbon for the effective removal of methylene blue from aqueous solution. *J. Clean. Prod.* **2016**, *115*, 337–342. [CrossRef]
13. Rashid, R.; Jawad, A.; Azlan, M.; Ishak, M.; Kasim, N. $FeCl_3$-activated carbon developed from coconut leaves: Characterization and application for methylene blue removal. *Sains Malays.* **2018**, *47*, 603–610. [CrossRef]
14. Pathania, D.; Sharma, S.; Singh, P. Removal of methylene blue by adsorption onto activated carbon developed from *Ficus carica* bast. *Arab. J. Chem.* **2017**, *10*, S1445–S1451. [CrossRef]
15. Wei, Y.; Fakudze, S.; Zhang, Y.; Ma, R.; Shang, Q.; Chen, J.; Liu, C.; Chu, Q. Co-hydrothermal carbonization of pomelo peel and PVC for production of hydrochar pellets with enhanced fuel properties and dechlorination. *Energy* **2022**, *239*, 122350. [CrossRef]
16. Tocmo, R.; Pena-Fronteras, J.; Calumba, K.F.; Mendoza, M.; Johnson, J.J. Valorization of pomelo (*Citrus grandis* Osbeck) peel: A review of current utilization, phytochemistry, bioactivities, and mechanisms of action. *Compr. Rev. Food Sci. Food Saf.* **2020**, *19*, 1969–2012. [CrossRef]
17. Liu, J.; Li, H.; Zhang, H.; Liu, Q.; Li, R.; Li, B.; Wang, J. Three-dimensional hierarchical and interconnected honeycomb-like porous carbon derived from pomelo peel for high performance supercapacitors. *J Solid State Chem.* **2017**, *257*, 64. [CrossRef]
18. Li, H.; Sun, Z.; Zhang, L.; Tian, Y.; Gui, G.; Yang, S. A cost-effective porous carbon derived from pomelo peel for the removal of methyl orange from aqueous solution. *Colloids Surf. A Physicochem. Eng. Asp.* **2016**, *489*, 191. [CrossRef]
19. Olivaresmarin, M.; Fernandezgonzalez, C.; Maciasgarcia, A.; Gomezserrano, V. Preparation of activated carbon from cherry stones by chemical activation with $ZnCl_2$. *Appl. Surf. Sci.* **2006**, *252*, 5967–5971. [CrossRef]
20. Wang, H.; Yan, T.; Shen, J.; Zhang, J.; Shi, L.; Zhang, D. Efficient removal of metal ions by capacitive deionization with straw waste derived graphitic porous carbon nanosheets. *Environ. Sci. Nano* **2020**, *7*, 317–326. [CrossRef]
21. Zhu, G.; Liu, Q.; Cao, F.; Qin, Q.; Jiao, M. Silkworm cocoon derived N, O-codoped hierarchical porous carbon with ultrahigh specific surface area for efficient capture of methylene blue with exceptionally high uptake: Kinetics, isotherm, and thermodynamics. *RSC Adv.* **2019**, *9*, 33872–33882. [CrossRef]
22. Zhang, S.; Zeng, M.; Li, J.; Li, J.; Xu, J.; Wang, X. Porous magnetic carbon sheets from biomass as an adsorbent for the fast removal of organic pollutants from aqueous solution. *J. Mater Chem.* **2014**, *2*, 4391–4397. [CrossRef]
23. Xian, F.; Gao, L.; Zhang, Z.; Zhang, H.; Dong, S.; Cui, G. N,P dual-doped multi-wrinkled nanosheets prepared from the egg crude lecithin as the efficient metal-free electrocatalyst for oxygen reduction reaction. *Appl. Surf. Sci.* **2019**, *476*, 76–83. [CrossRef]
24. Zou, J.; Dai, Y.; Liu, D.; Wang, S.; Zhou, L.; Zhou, Y. Synthesis of carboxyl-functionalized magnetic nanoparticle for the removal of methylene blue. *Colloid Surf. A Physicochem. Eng. Asp.* **2019**, *572*, 58–66.
25. Ozdemir, I.; Şahin, M.; Orhan, R.; Erdem, M. Preparation and characterization of activated carbon from grape stalk by zinc chloride activation. *Fuel Process. Technol.* **2014**, *125*, 200–206. [CrossRef]
26. Singh, R.; Pal, D.; Mathur, A.; Singh, A.; Krishnan, M.A.; Chattopadhyay, S. An efficient pH sensitive hydrogel, with biocompatibility and high reusability for removal of methylene blue dye from aqueous solution. *React. Funct. Polym.* **2019**, *144*, 104346. [CrossRef]

27. Zhang, C.; Li, P.; Huang, W.; Cao, B. Selective adsorption and separation of organic dyes in aqueous solutions by hydrolyzed PIM-1 microfibers. *Chem. Eng. Res. Des.* **2016**, *109*, 76–85. [CrossRef]
28. Dai, J.; Sun, J.; Xie, A.; He, J.; Li, C.; Yan, Y. Designed preparation of 3D hierarchically porous carbon material via solvothermal route and in situ activation for ultrahigh-efficiency dye removal: Adsorption isotherm, kinetics and thermodynamics characteristics. *RSC Adv.* **2016**, *6*, 3446–3457. [CrossRef]
29. Nasrullah, A.; Saad, B.; Bhat, A.; Khan, A.S.; Danish, M.; Isa, M.H.; Naeem, A. Mangosteen peel waste as a sustainable precursor for high surface area mesoporous activated carbon: Characterization and application for methylene blue removal. *J. Clean. Prod.* **2019**, *211*, 1190–1200. [CrossRef]
30. Shen, X.; Huang, P.; Li, F.; Wang, X.; Yuan, T.; Sun, R. Compressive alginate sponge derived from seaweed biomass resources for methylene blue removal from wastewater. *Polymers* **2019**, *11*, 961. [CrossRef]
31. Cheng, S.; Zhang, L.; Ma, A.; Xia, H.; Peng, J.; Li, C.; Shu, J. Comparison of activated carbon and iron/cerium modified activated carbon to remove methylene blue from wastewater. *J. Environ. Sci.* **2018**, *65*, 92–102. [CrossRef]
32. Jin, Q.; Li, Y.; Yang, D.; Cui, J. Chitosan-derived three-dimensional porous carbon for fast removal of methylene blue from wastewater. *RSC Adv.* **2018**, *8*, 1255–1264. [CrossRef]
33. Kang, Y.; Wei, X.; Liu, G.; Mu, M.; Ma, X.; Gao, Y.; Zong, Z. CO_2-hierarchical activated carbon prepared from coal gasification residue: Adsorption equilibrium, isotherm, kinetic and thermodynamic studies for methylene blue removal. *Chin. J. Chem. Eng.* **2020**, *28*, 1694–1700. [CrossRef]
34. Ladshaw, A.; Yiacoumi, S.; Lin, R.; Nan, Y.; Tavlarides, L.L.; Tsouris, C. A mechanistic modeling framework for gas-phase adsorption kinetics and fixed-bed transport. *AIChE J.* **2017**, *63*, 5029–5043. [CrossRef]
35. Li, X.; Han, D.; Xie, J.; Wang, Z.; Gong, Z.; Li, B. Hierarchical porous activated biochar derived from marine macroalgae wastes (*Enteromorpha prolifera*): Facile synthesis and its application on Methylene Blue removal. *RSC Adv.* **2018**, *8*, 29237–29247. [CrossRef]
36. Wang, Z.; Xu, D.; Xu, J.; Zhang, L.; Zhang, X. Graphene oxide gel-derived, free-Standing, hierarchically porous carbon for high-capacity and high-rate rechargeable LiO_2 batteries. *Adv. Funct. Mater.* **2012**, *22*, 3699–3705. [CrossRef]
37. Kim, K.; Park, S. Synthesis and electrochemical performance of well-balanced mesopore/micropore contained carbons by activation-free method. *Electrochem. Commun.* **2012**, *22*, 89–92. [CrossRef]
38. Xu, F.; Cai, R.; Zeng, Q.; Zou, C.; Wu, D.; Li, F.; Liu, X.; Liang, Y.; Fu, R. Fast ion transport and high capacitance of polystyrene-based hierarchical porous carbon electrode material for supercapacitors. *J. Mater. Chem.* **2011**, *21*, 1970–1976. [CrossRef]
39. Peng, X.; Huang, D.; Odoomwubah, T.; Fu, D.; Huang, J.; Qin, Q. Adsorption of anionic and cationic dyes on ferromagnetic ordered mesoporous carbon from aqueous solution: Equilibrium, thermodynamic and kinetics. *J. Colloid Interf. Sci.* **2014**, *430*, 272–282. [CrossRef]
40. Jiang, H.; Wang, Y.; Hao, J.; Liu, Y.; Li, W.; Li, J. N and P co-functionalized three-dimensional porous carbon networks as efficient metal-free electrocatalysts for oxygen reduction reaction. *Carbon* **2017**, *122*, 64–73. [CrossRef]
41. Wang, Z.; Tan, Y.; Yang, Y.; Zhao, X.; Liu, Y.; Niu, L.; Tichnell, B.; Kong, L.; Kang, L.; Liu, Z.; et al. Pomelo peels-derived porous activated carbon microsheets dual-doped with nitrogen and phosphorus for high performance electrochemical capacitors. *J. Power Sources* **2018**, *378*, 499–510. [CrossRef]
42. Basaleh, A.A.; Almalack, M.H.; Saleh, T.A. Methylene Blue removal using polyamide-vermiculite nanocomposites: Kinetics, equilibrium and thermodynamic study. *J. Environ. Chem. Eng.* **2019**, *7*, 103107. [CrossRef]
43. Zhang, W.; Zhang, L.Y.; Zhao, X.J.; Zhou, Z. Citrus pectin derived ultrasmall Fe_3O_4@C nanoparticles as a high-performance adsorbent toward removal of methylene blue. *J. Mol. Liq.* **2016**, *222*, 995–1002. [CrossRef]
44. Liu, F.; Zou, H.; Hu, J.; Liu, H.; Peng, J.; Chen, Y.; Lu, F.; Huo, Y. Fast removal of methylene blue from aqueous solution using porous soy protein isolate based composite beads. *Chem. Eng. J.* **2016**, *287*, 410–418. [CrossRef]
45. Islam, M.A.; Ahmed, M.J.; Khanday, W.A.; Asif, M.; Hameed, B.H. Mesoporous activated carbon prepared from NaOH activation of rattan (*Lacosperma secundiflorum*) hydrochar for methylene blue removal. *Ecotox. Environ. Safe.* **2017**, *138*, 279–285. [CrossRef]
46. Lu, Q.; Li, Q.; Zhang, J.; Li, J.; Lu, J. Facile mesoporous template-assisted hydrothermal synthesis of ordered mesoporous magnesium silicate as an efficient adsorbent. *Appl. Surf. Sci.* **2016**, *360*, 889–895. [CrossRef]
47. Gan, W.; Shang, X.; Li, X.; Zhang, J.; Fu, X. Achieving high adsorption capacity and ultrafast removal of methylene blue and Pb^{2+} by graphene-like TiO_2@C. *Colloids Surf. A Physicochem. Eng. Asp.* **2019**, *561*, 218–225. [CrossRef]